Influence of the multiscale distribution of particles on elastic properties of concrete

Julie Escoda[a], François Willot[1a], Dominique Jeulin[a], Julien Sanahuja[b], Charles Toulemonde[b]

[a]*MINES ParisTech, PSL - Research university, Centre for Mathematical Morphology*
35, rue St Honoré, F-77300 Fontainebleau, France
[b]*Département Matériaux et Mécanique des Composants, Électricité de France, Moret-sur-Loing, France*

Published in *International Journal of Engineering Science* 98, 60–71 (2016).
The final publication is available at Elsevier via `http://dx.doi.org/10.1016/j.ijengsci.2015.07.010`

Abstract

The mechanical role of the shape of the aggregates, and their spatial distribution in concrete materials is examined. The effect on the macroscopic mechanical response as well as on the local stress fields are investigated by numerical means, making use of a recently developed Poisson-polyhedra model in which the aggregates have polyhedral shapes. Comparison is made with previous microstructure models of spheres. Full-field computations are carried out on large volume size using Fourier methods. The field maps are used to determine zones of highest stress. Furthermore, the scale separation hypothesis for the computation of the elastic properties is investigated using numerical calculations on various multiscale microstructures. Finally, numerical predictions for the elastic properties are compared to experimental measurements, and the results discussed.

Keywords: FFT methods, Homogenization, Concrete, Multiscale microstructures, Linear elasticity

1. Introduction

Tools for the prediction of the mechanical behavior of concrete from its microstructure become more and more available (Chunsheng et al., 2014, He et al., 2011) and progressively give access to the design of new formulations in order to improve its behavior (Shilstone, 1990). The presence of a very wide range of sizes for gravels with random shapes (covering from 5 μm up to 12.5 mm) makes the description of the morphology of concrete a real challenge for a numerical prediction of concrete's effective properties. Such a range of sizes makes practically inaccessible a 3D investigation of concrete specimens by means of techniques like CT microtomography. Another consequence of these multiple scales in concrete is the difficulty to produce meshes suitable for the implementation of a finite elements code in order to predict its effective properties. For these reasons, we developed a chain of tools to produce virtual 3D samples of concrete and to predict its elastic properties. Based on iterative calculations involving the use of Fast Fourier Transform (Willot, 2015, Escoda et al., 2011c, Escoda et al., 2011b), it predicts the elastic fields generated under appropriate sollicitations. and gives access to the effective behavior and to detailed maps of the stress and stain states inside the concrete specimen. This information can be used to improve the elastic properties of concrete, and also to detect possible sites of stress and strain concentrations that could initiate damage.

The present study focuses on the "Biloba" concrete, described in Section (2). The latter also presents a microstructure model made of random Poisson polyhedra, proposed in previous works (Escoda et al., 2011a, Escoda, 2012, Escoda et al., 2015), which is extensively used afterwards. Experimental measurements for the Biloba concrete's elastic response are also given. Sections (3) and (4) examine the influence of shape of the aggregates on the elastic properties and to which extent the scale separation hypothesis holds. Experimental measurements and numerical predictions are compared in Section (5). Concluding remarks are given in Section (6).

[1]Corresponding author, email: `francois.willot@ensmp.fr`. Tel.: +33 1 64 69 48 07. ©2015. This manuscript version is made available under the CC-BY-NC-ND 4.0 license `http://creativecommons.org/licenses/by-nc-nd/4.0/`

2. "Biloba" concrete

This study focuses on the modeling of the "Biloba" concrete (Legrix, 2009). The Biloba concrete has been fabricated by EDF R&D to reproduce closely a type of concrete, called "B11", used in the reactor containment of the power plant of Civaux, France (Granger, 1996). It is composed of sand, gravels and cement. Hereafter, we will refer to both sand and gravels as "aggregates". The cement is a Portland cement manufactured by the company Calcia in Airvault, France, of type CEM-II/A-LL 42.5-R-CE PM-CP2-NF and specific surface 3810 cm^2g^{-1}. The aggregates have been obtained by crushing rocks excavated from the quarry of Saint-Maurice-la-Clouère, France. The aggregates have continuously-increasing size distribution, and are supplied in three separate classes: sand ($0-4$ mm), fine gravels ($4-12.5$ mm) and gravels ($10-20$ mm). Hereafter, as sand particles with a diameter smaller than 0.1 mm have size order of that of the cement, they are incorporated in the phase we will referred to as "cement paste". The latter is modeled as a homogeneous phase. Accordingly, sand will refer to the sand particles larger than 0.1 mm. In the Biloba sand has been sieved to obtain a granulometry curve close to that of the "B11" concrete. Granulometry curves have been experimentally measured by the company Ginger CEBTP (norm NF EN 933) for the two classes of gravels and by EDF (Legrix, 2009) for the sand. The volume fractions of each of the three classes are 25.9% (sand), 12.3% (fine gravels) and 30.5% (gravels) and the total volume fraction of aggregates is accordingly 68.7% (Escoda, 2012). A sample of the Biloba concrete is visible in Fig. (1). In this figure, the size of the largest aggregates is about 1.2 cm.

2.1. Microstructure models

The present study relies on a Poisson-polyhedra microstructure model developed in previous works (Escoda et al., 2011a, Escoda et al., 2015) for the the Biloba concrete. In this model, the gravels and sand are polyhedra which lie in the complementary set of a tesselation of Poisson planes. The tesselation is defined by a Poisson intensity λ, or number of planes per unit volume. We denote by "Poisson polyhedra", the polyhedra generated by such a tesselation, of which one useful measurement is their granulometry. The granulometry of the Biloba concrete is well approximated by a combination of three truncated granulometries of Poisson polyhedra (Escoda et al., 2015). Truncated granulometries consist in the set of Poisson polyhedra with minimum and maximum diameter. The latter are used in the model to obtain a multi-scale microstructure. The microstructure is simulated by sequentially implanting Poisson polyhedra, starting with the largest ones, in a volume, until the required volume fractions for each of the three classes is obtained. No overlap occurs in the packing process. The polyhedra are defined vectorially, but the resulting microstructure is discretized on a grid of voxels, or image.

The model accordingly makes use of 4 parameters for each class of aggregates: the minimum and maximum diameters for the truncated granulometry, the Poisson intensity and the volume fraction. For the packing of the aggregates, an additional size parameter, ω, expressed in voxels, is used to control the displacement of the aggregates during implantation (see Escoda et al., 2015). Following (Escoda et al., 2015), the value of ω is set to 2 voxels. The three truncated granulometries in the model do not overlap and are defined by the following ranges (Escoda et al., 2015): 0.05–2.4 mm, 2.4–6.15 and 6.15–12.5 mm. They are denoted class 1, 2 and 3 respectively. We denote by λ_i and f_i ($i = 1, 2, 3$) the Poisson intensity (mm^{-1}) and volume fraction of each class of aggregates. The total volume fraction of the aggregates is denoted f_t. We emphasize that in all models considered in this work, the cement paste does percolate whereas the aggregates do not.

2.2. Elastic properties

The Young modulus of the Biloba concrete, determined experimentally, is $E^{\mathrm{b}} = 28.7 \pm 1.4$ GPa. The confidence interval is given by the standard deviation obtained on three measurements (Escoda, 2012). A value of $\nu^{\mathrm{b}} = 0.22$ is provided for the Poisson ratio of the Biloba concrete in (Reviron, 2009).

The elastic moduli of the aggregates and cement paste in the Biloba concrete have not been directly measured. Nevertheless data provided in (Granger, 1996) and (Wrigers & Moftah, 2006) indicates a value of about $\nu^{\mathrm{c}} \approx \nu^{\mathrm{g}} \approx 0.2$ for the Poisson ratios of both the cement paste and aggregates. The cement paste in the "B11" concrete is similar to that used in the Biloba concrete. Its modulus, measured in (Granger, 1996), is 18.0 GPa. Hereafter, we adopt the value $E^{\mathrm{c}} = 20.0$ GPa (see (Escoda, 2012)) for the cement paste. The Young modulus of the aggregates E^{g} is given by the contrast of properties χ:

$$\chi = \frac{E^{\mathrm{g}}}{E^{\mathrm{c}}}. \tag{1}$$

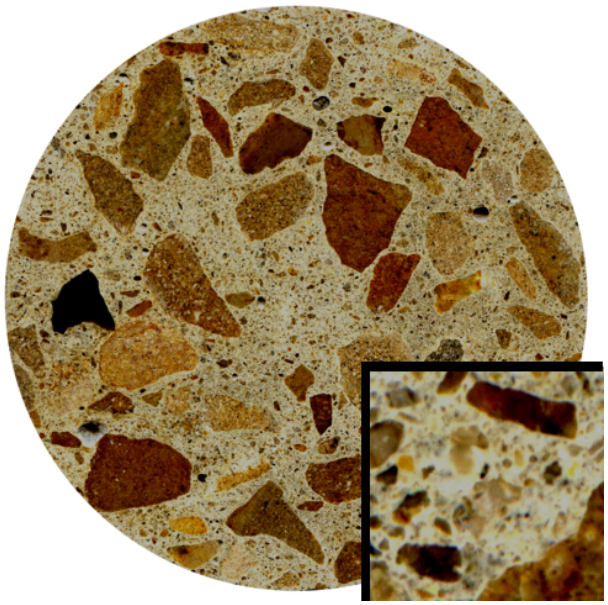


Figure 1: "Biloba" concrete sample of diameter 11 cm (image obtained using an image scanner). Bottom-right: 20× magnification.

In the rest of this work, the following value is used: $\chi = 3$ or equivalently $E^{\mathrm{g}} = 60$ GPa. This level of contrast is consistent with the data in (Granger, 1996) and (Wrigers & Moftah, 2006). For the "B11" concrete, for instance, measurement of the Young modulus of the aggregates gives 61.4 GPa.

In the present work, a higher contrast of properties is explored, namely $\chi = 100$. This is done by fixing $E^{\mathrm{c}} = 20.0$ and letting E^{c} takes on values 100 times higher than E^{c}. The reason for this choice is given in (Sanahuja & Toulemonde, 2011). In this work, the viscoelastic response of concrete is re-written as a set of linear elastic problems with varying contrast of properties. The long-term response of the material, in the range of $10 - 100$ years, is driven by a set of elastic problems with much stiffer aggregates than in reality. The contrast of properties of the corresponding elastic moduli varies from 11 to 317 (Sanahuja & Toulemonde, 2011). Thus the choice $\chi = 100$ allows one to evaluate the effect of microstructure on the mechanical properties of concrete. Obviously, the effect of microstructure should be much stronger for such level of contrast, in agreement with previous observations for the long-term creep response of concrete (Sanahuja & Toulemonde, 2011). Full-field viscoelastic computations are needed for more quantitative studies. The latter is however outside of the present study, and is left to future work. The bulk and shear moduli are readily determined from the experimental Young modulus and Poisson ratio. They are denoted by $\kappa^{b,c,g}$ and $\mu^{b,c,g}$. The superscript b, c and g refer to the (macroscopic) Biloba concrete, cement paste and aggregates, respectively.

In the rest of this work, the following notations are adopted: the displacement, strain and stress fields at point $\boldsymbol{x}$ are denoted $\mathbf{u}(\boldsymbol{x})$, $\boldsymbol{\varepsilon}(\boldsymbol{x})$ and $\boldsymbol{\sigma}(\boldsymbol{x})$ respectively. They satisfy:

$$\partial_i \sigma_{ij} \equiv 0, \quad \varepsilon_{kl} = (1/2)(\partial_k u_l + \partial_l u_k), \quad \sigma_{ij}(\boldsymbol{x}) = C_{ij,kl}(\boldsymbol{x})\varepsilon_{kl}(\boldsymbol{x}), \tag{2}$$

where $C_{ij,kl}(\boldsymbol{x})$ is the (isotropic) elastic stiffness tensor of the phase at point $\boldsymbol{x}$. Cartesian coordinates along axis $\mathbf{e}_i$ ($i = 1$, 2, 3) are used for all tensor fields. The mean stress components is denoted by the subscript m, i.e. $\sigma_m = (1/3)\sigma_{ii}$. Likewise, $\varepsilon_m = (1/3)\varepsilon_{kk}$.

The "augmented Lagrangian" numerical Fourier method in (Michel et al., 2000) is used to solve the above elasticity problem subjected to a macroscopic strain loading $\boldsymbol{\varepsilon}^0$:

$$\langle \varepsilon_{ij} \rangle = \varepsilon^0_{ij}. \tag{3}$$

In the above, $\langle \cdot \rangle$ refers to spatial means over the computational domain. We recall that periodic boundary conditions are applied over the boundaries of the domain in the Fourier method (Michel et al., 2000). The Fourier computations

Class	2	3
λ_i (mm^{-1})	0.0418	0.0695
f_i	0.29	0.12
Resolution (mm/voxel)	0.24	
Image size	1024^3 (24.6^3 cm^3)	
f_t	0.40	

Table 1: Parameters used to generate a polyhedra microstructure resembling the simplified sphere model of the B11 concrete used in (Dunant et al., 2013), and essential geometrical descriptors.

are carried out using the microscopic elastic moduli $\kappa^{c,g}$ and $\mu^{c,g}$ as inputs. The effective bulk and shear moduli, predicted by the numerical computations are denoted $\widetilde{\kappa}$ and $\widetilde{\mu}$. The latter are compared to the measured moduli κ^b and μ^b. The effective stiffness tensor with elastic moduli $\widetilde{\kappa}$ and $\widetilde{\mu}$ is denoted $\widetilde{C}$. The components of $\widetilde{C}_{ij,kl}$ are computed by measuring appropriate means of the stress field. For instance, $\widetilde{C}_{11,11}$ is derived from the mean $\langle\sigma_{11}(\boldsymbol{x})\rangle$ when $\varepsilon^0_{11} = 100\%$ and all other components are set to zero. Hereafter, the following loadings:

$$\varepsilon^0_{ij} = \delta_{ij}, \qquad \varepsilon^0_{ij} = (\delta_{i1}\delta_{j2} + \delta_{i2}\delta_{j1}), \tag{4}$$

are referred to as hydrostatic and, by convention, shear strain loadings, respectively.

3. Influence of the particles shape

3.1. Polyhedra and spheres microstructure models

In this section, we consider a microstructure model made of an assembly of 2024 spheres. The spheres are well separated, i.e. they do not interpenetrate. This microstructure has been used as a benchmark for computational mechanics methods in (Dunant et al., 2013), where it is referred to as "B11" concrete. The spheres model is a simplified representation of the largest aggregates (> 2 mm) in the Biloba concrete. The distribution of diameters of the spheres follow the granulometry of the two largest aggregates classes.

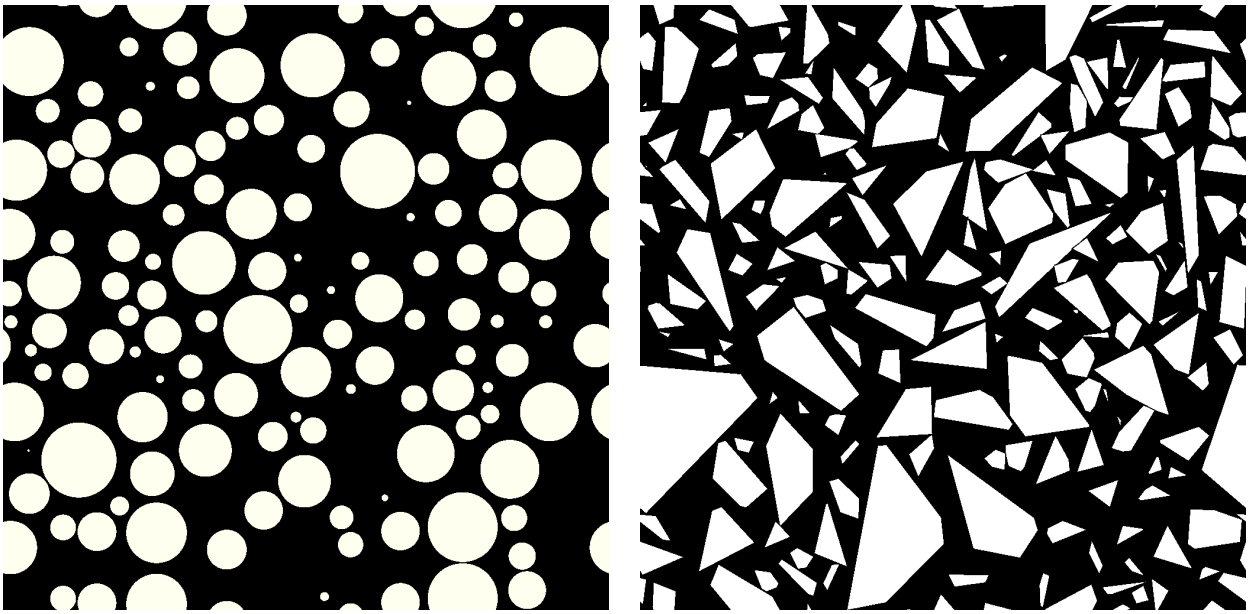
To evaluate the effect of particle shape on the elastic properties, a second microstructure model is considered, which is made of polyhedra instead of spheres. The parameters used to generate the Poisson-polyhedra model are given in Table (1). As for the spheres, the model mimics the granulometry of the largest aggregates. The polyhedra are implanted in a 3D volume, without interpenetration. Their size distribution is a combination of two truncated Poisson polyhedra distributions which are specified by two Poisson intensities. As detailed in (Escoda et al., 2015), the two truncated Poisson polyhedra distributions approximate the granulometry of the two largest aggregates classes. The total volume fraction of the aggregates in the polyhedra model is 40.3%, close to that obtained in the spheres model, of 40.2%. Furthermore, the number of polyhedra and spheres implanted in the two models is of the same order. For illustration, 2D sections of the spheres and polyhedra models are represented in Fig. (2).

3.2. Elastic response

The local and effective elastic response of the spheres and polyhedra models are determined numerically. Stiff inclusions are assumed, i.e. $\chi = 100$. Full-field maps of the stress components $\sigma_m(\boldsymbol{x})$ and $\sigma_{12}(\boldsymbol{x})$ are shown in Fig. (3) in a 2D section parallel to the $(\mathbf{e}_1, \mathbf{e}_2)$ plane. The latter correspond to, respectively, hydrostatic and shear strain loading, so that the stress components represented are "parallel" to the applied strain field, and have non-zero mean.

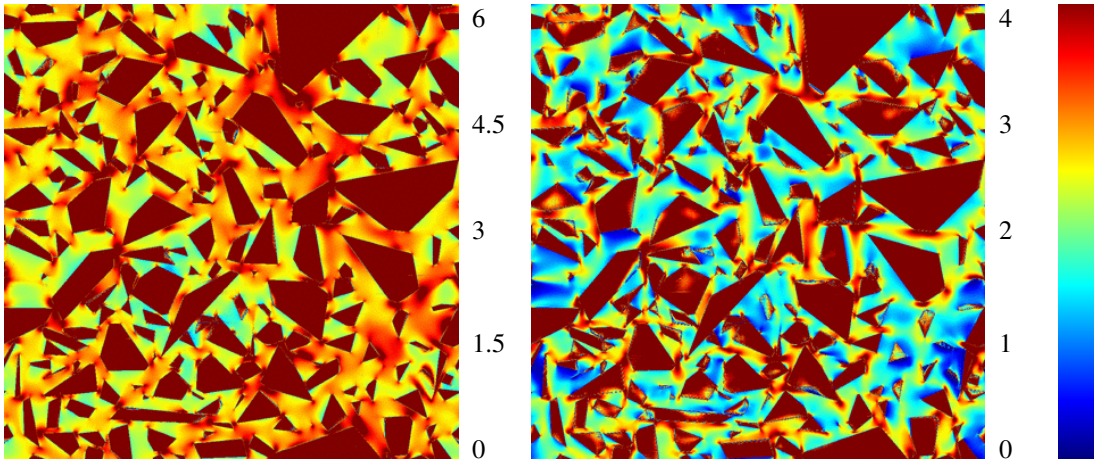
The corresponding histograms $P_{\sigma_{12,m}}$ of the stress components in the cement paste are represented in Fig. (4). The quantity $P_{\sigma_{12,m}}(t)\mathrm{d}t$ is equal to the probability that $t \leq \sigma_{12,m}(\boldsymbol{x}) \leq t + \mathrm{d}t$ holds knowing that $\boldsymbol{x}$ is in the cement paste. All distributions are asymmetric and clearly non-Gaussian. On average, the stress fields in the cement paste is also much higher for the Poisson-polyhedra model than it is for the spheres models. This result is somehow expected as the sphere model is closer to the Hashin spheres assemblage, with lowest elastic moduli, than the polyhedra model. In contrast, the aggregates in the polyhedra model tend to be closer to each other than in the spheres model.

Histograms tails are represented in log-log plot in the top-right quadrant in Fig. (4). The latter decrease to 0 with a similar rate $\sim t^\beta$ for $t \gg 1$ and $\beta < 0$ for the spheres and polyhedra model, and for the two types of loadings. This is



(a) (b)

Figure 2: 2D sections of the spheres (a) and Poisson polyhedra (b) models that simulate the "Biloba" concrete, with aggregates from class 2 and 3 only. Model (b) is generated according to the parameters given in Table (1).



(a) (b)

Figure 3: 2D sections of the stress components σ_m (a) and σ_{xy} (b) with hydrostatic strain loading $\langle \varepsilon_m \rangle = \varepsilon_0 = 100\%$ and $\langle \varepsilon_{xy} \rangle = \varepsilon_0 = 100\%$ resp. for the polyhedra model. The color scale indicated on the right has been chosen to highlight the fields's features in the matrix.

consistent with previous results obtained using computational methods on a segmented microtomography image of a mortar material (Escoda et al., 2011c, Escoda et al., 2011b).

The means of the two stress components σ_m and σ_{12} in the cement paste are plotted as a function of the distance to the aggregates and to the SKIZ in Fig. (5). The distance to the aggregate or SKIZ is computed using a pseudo-Euclidean distance function (Soille, 1994). The SKIZ is the skeleton by influence zone of the aggregates (Lantuéjoul, 1980), and consists of surfaces located in-between the aggregates (see e.g. (Escoda et al., 2011c)). Highest values of the stress components are obtained closer to the aggregates-cement paste interface. Note that the oscillations for the statistics

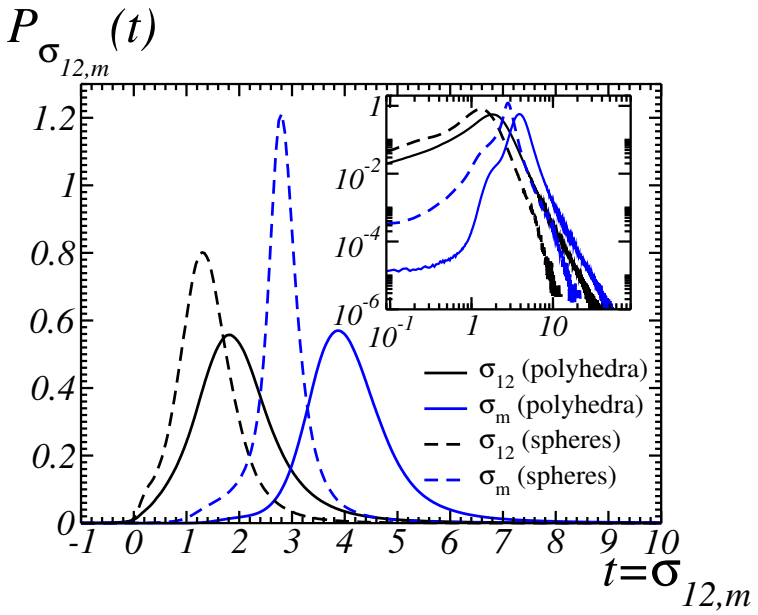


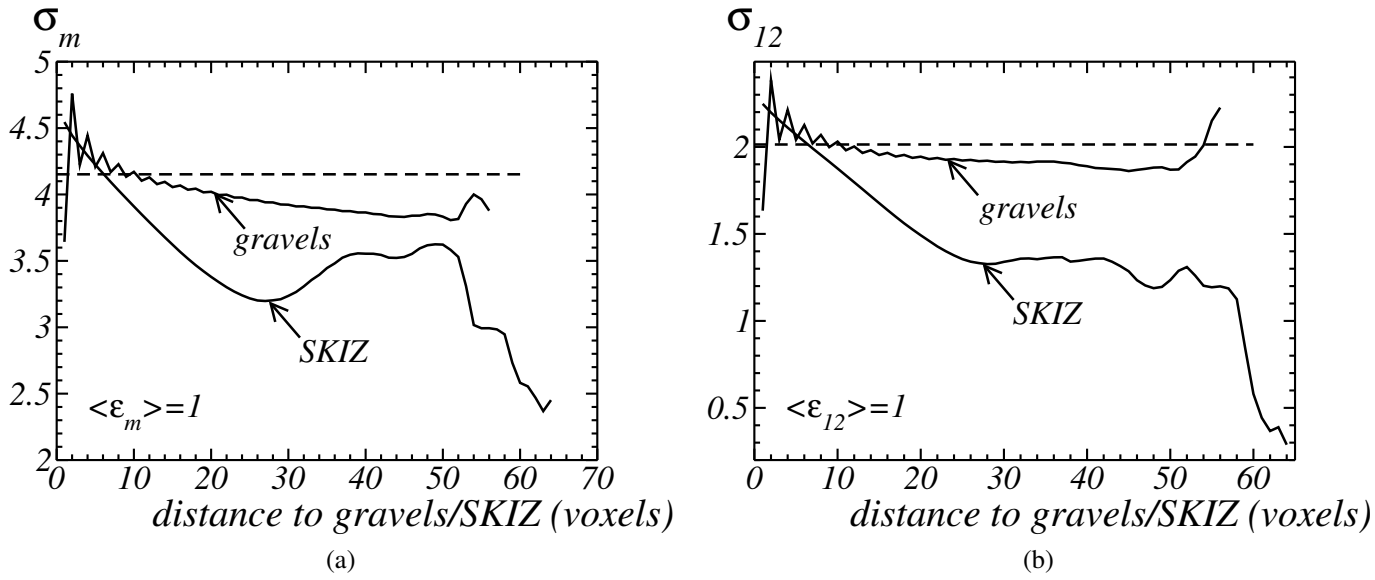
Figure 4: Histograms $P_{\sigma_{12,m}}$ of the shear and mean stress components σ_{12} (black) and σ_m (blue) in the cement paste, with applied shear and hydrostatic strain loading $\langle\varepsilon_{12}\rangle = \varepsilon_0 = 100\%$ and $\langle\varepsilon_m\rangle = \varepsilon_0 = 100\%$ resp.: spheres model (dotted lines) and Poisson-polyhedra model (solid lines). The fields averages in the cement paste are $\langle\sigma_m\rangle_c = 2.8$ (spheres), 4.2 (polyhedra) and $\langle\sigma_{12}\rangle_c = 1.4$ (spheres), 2.0 (polyhedra). Top-right plot: distribution tails in log-log scales.

close to the interface are presumably an effect of the FFT discretization (Willot, 2015). In another study focusing on granular media (Willot et al., 2013), the highest field values were found to lie along the gaps of nearly-touching stiff inclusions. This is consistent with the results obtained in this work. However, for polyhedra aggregates, one must also consider singularities of the stress fields at the corners of the inclusions. Highest stress fields are also found in zones close to the SKIZ, which must pass in-between aggregates that are close to one another. Again, this result is consistent with a previous study on mortar (Escoda et al., 2011c).

Effective elastic moduli are given in Table (2) and compared to Hashin and Shtrikman's bounds (Hashin & Shtrikman, 1963) for the bulk and shear moduli, denoted $\kappa^{\pm}_{HS}$. and $\mu^{\pm}_{HS}$ respectively. Note that the equality $\kappa^{\pm}_{HS} = \mu^{\pm}_{HS}$ is a fortuitous consequence of the equality $\nu^g = \nu^c = 0.2$. The representative volume element (RVE) for a required relative precision of the bulk and shear moduli of 5% are denoted by $V^{\kappa,\mu}_{5\%}$. The two are computed for the polyhedra microstructure from the variance of the apparent moduli estimated over subdomains of the microstructure. The method, not described here, is detailed in (Kanit et al., 2003). In addition, the variances $\langle\sigma^2_{12,m}\rangle_c - \langle\sigma_{12,m}\rangle^2_c$, extracted from the FFT maps, are given in Table (2) as well as the effective modulus $\widetilde{C}_{11,11}$ which is computed in (Dunant et al., 2013).

The RVE size for a precision of 5% are noticeably lower than the computations performed here, for which the precision is better than 1%. The polyhedra model generates higher extremal values of the stresses, which might involve a higher sensitivity to the development of local damage in the microstructure. Both bulk and shear moduli lie in-between the Hashin and Shtrikman bounds, but are closer to the lower bound. Despite the difference in the stress field histograms observed in Fig. (4) for the polyhedra and spheres models, the bulk modulus is nearly insensitive to the microstructure. The field variances in the cement paste, however, are notably different. Consistently with previous observations regarding the tails of the histograms P_{σ_m}, the variances for the bulk and shear moduli are much higher for the polyhedra model than the spheres model.

The shear modulus for the polyhedra model is, however, about 12% higher than for the spheres model. This is presumably the result of the anisotropy of the aggregates. The shear modulus is accordingly more sensitive to the elongation and shape of the aggregates. The increase for the modulus $\widetilde{C}_{11,11}$, involving both shear and bulk moduli, is intermediate: it is about 8% higher for the polyhedra model compared to the spheres model.



(a) (b)

Figure 5: Mean of the stress components σ_m (a) and σ_{12} (b) in the cement paste as a function of the distance to aggregates for the Poisson-polyhedra model. The material is subjected to hydrostatic strain loading $\varepsilon^0_m = 100\%$ (a) and shear loading $\varepsilon^0_{12} = 100\%$ (b). The distance on the x-axis is computed by propagating the pseudo-Euclidean distance function from the aggregates-cement interface or from the SKIZ of the aggregates. Straight horizontal lines: average of the stress components σ_m and σ_{12} in the matrix.

4. Scale-separation assumption

4.1. Two-scales and three-scales microstructure models

This section is devoted to the validity of the scale-separation assumption. More precisely, two methods for estimating the elastic response of the Biloba concrete are considered. Again, a contrast of properties of $\chi = 100$ is assumed between the aggregates and the cement paste. The first one simply uses the full three-scales model for the Biloba concrete which is proposed in (Escoda et al., 2015). It contains the three classes of aggregates 0.05–2.4 mm, 2.4–6.15 and 6.15–12.5 mm. FFT computations are carried out on the microstructure model for estimating the elastic properties. Examples of FFT maps for the strain and stress fields are shown in Figs. (8) and (9). This method, however, necessitates CPU and memory-intensive computations. The resolution should be fine enough to capture sand particles and the image size large enough to contain a sufficient amount of large aggregates.

The Poisson intensities and prescribed volume fractions of classes 1, 2 and 3 of aggregates are $\lambda_1 = 0.518$, $\lambda_2 = 0.0695$, $\lambda_3 = 0.0418$ mm^{-1} and $f_1 = 24\%$, $f_1 = 12.3\%$ and $f_3 = 30.5\%$, respectively. The microstructure size is 1600^3 voxels or 14.4^3 cm^3 with resolution 0.09 mm/voxel. The final volume fraction of aggregates is 64.3%. A 2D section of the model is represented in Fig. (7).

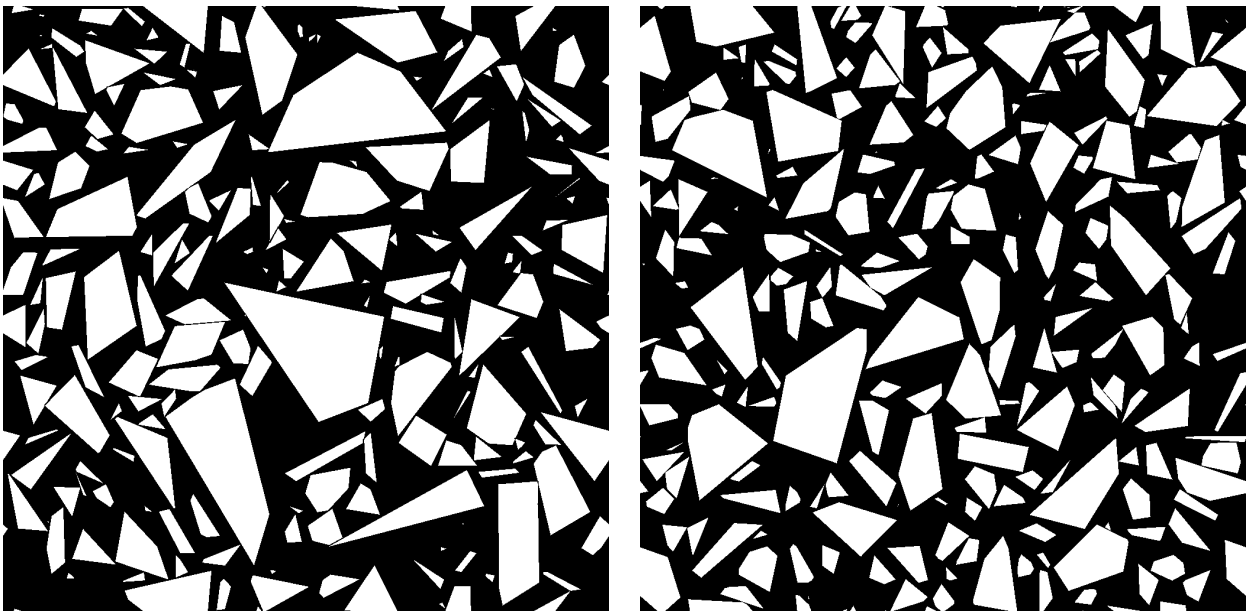
The second method makes use of two microstructures and two FFT computations. First, a sand-cement microstructure is used. It contains sand, the smallest class of aggregates, embedded in the cement paste with contrast of properties of $\chi = 100$. The volume fraction of aggregates is determined from the three-scales microstructures given in (Escoda et al., 2015). This is the volume fraction of the smallest class of aggregates relative to the complementary set of the two largest class. The latter is also the union of the cement paste and of the smallest class of aggregate. In the second step, the three-scales microstructure is used, but the sand and cement paste are replaced by a homogeneous phase with properties equal to the effective elastic response previously computed for the sand-cement microstructure. This methodology becomes exact when the sand particle sizes are much lower than that of the other aggregates, i.e. when scale separation can be assumed. This is however not the case for the Biloba concrete. The second methodology has an obvious advantage in terms of computational costs, since it requires much lower resolution for the two computations than in the first method.

The sand-cement microstructure in the second method was generated with a Poisson intensity $\lambda_1 = 0.52$ mm^{-1} and volume fraction for the sand of $f_1 = 43.0\%$. The microstructure size is 1024^3 voxels or 15.4^3 cm^3 with resolution 0.015

Microstructure	B11-polyhedra model	B11-spheres model
$\widetilde{\kappa}/\kappa^c$	3.16	3.17
κ^+_{HS}/κ^c	26.2	
κ^-_{HS}/κ^c	2.3	
$V^{\kappa}_{5\%}$	8.6^3 cm^3 (336^3 voxels)	–
$\langle\sigma^2_m\rangle_c - \langle\sigma_m\rangle^2_c$	1.30	0.43
$\widetilde{\mu}/\mu^c$	3.52	3.14
μ^+_{HS}/μ^c	26.2	
μ^-_{HS}/μ^c	2.3	
$V^{\mu}_{5\%}$	9.4^3 cm^3 (394^3 voxels)	–
$\langle\sigma^2_{12}\rangle_c - \langle\sigma_{12}\rangle^2_c$	1.00	0.39
$\widetilde{C}_{11,11}/C^c_{11,11}$	3.34	3.11

Table 2: Effective elastic properties of the polyhedra and spheres simplified models for the B11 concrete: elastic moduli $\widetilde{\kappa}, \widetilde{\mu}$ and $\widetilde{C}_{11,11}$, Hashin and Shtrikman bounds $\kappa^{\pm}_{HS}$, $\mu^{\pm}_{HS}$, stress field second-moments in the cement paste $\langle\sigma^2_{12,m}\rangle_c$ and representative volume element for a required relative precision of 5%.

mm/voxel. The second microstructure, containing aggregates of classes 2 and 3 embedded in an equivalent medium, was generated using the Poisson intensities $\lambda_2 = 0.0695$, $\lambda_3 = 0.0418$ mm^{-1} with respective volume fractions $f_2 = 12.3$ and $f_3 = 30.5\%$. The microstructure size is 1024^3 voxels or 24.6^3 cm^3 with resolution 0.24 mm/voxel. Random 2D sections of the sand-cement microstructure and that with the aggregates of classes 2 and 3 are represented in Fig. (6).



(a) (b)

Figure 6: 2D sections of the microstructures used in the computations assuming scale-separation: (a) sand-cement microstructure, (b) microstructure with the two largest classes of aggregates embedded in an equivalent model (in grey) determined from (a). The microstructure in (b) is represented at a much lower scale than that in (a).

4.2. Elastic response

For the 3-scales model, the microstructure resolution of 0.09 mm/voxel was insufficient to discretize the smallest aggregates, with size as low as 0.05 mm. The volume fraction of sand is accordingly 24%, instead of 25.9% for the

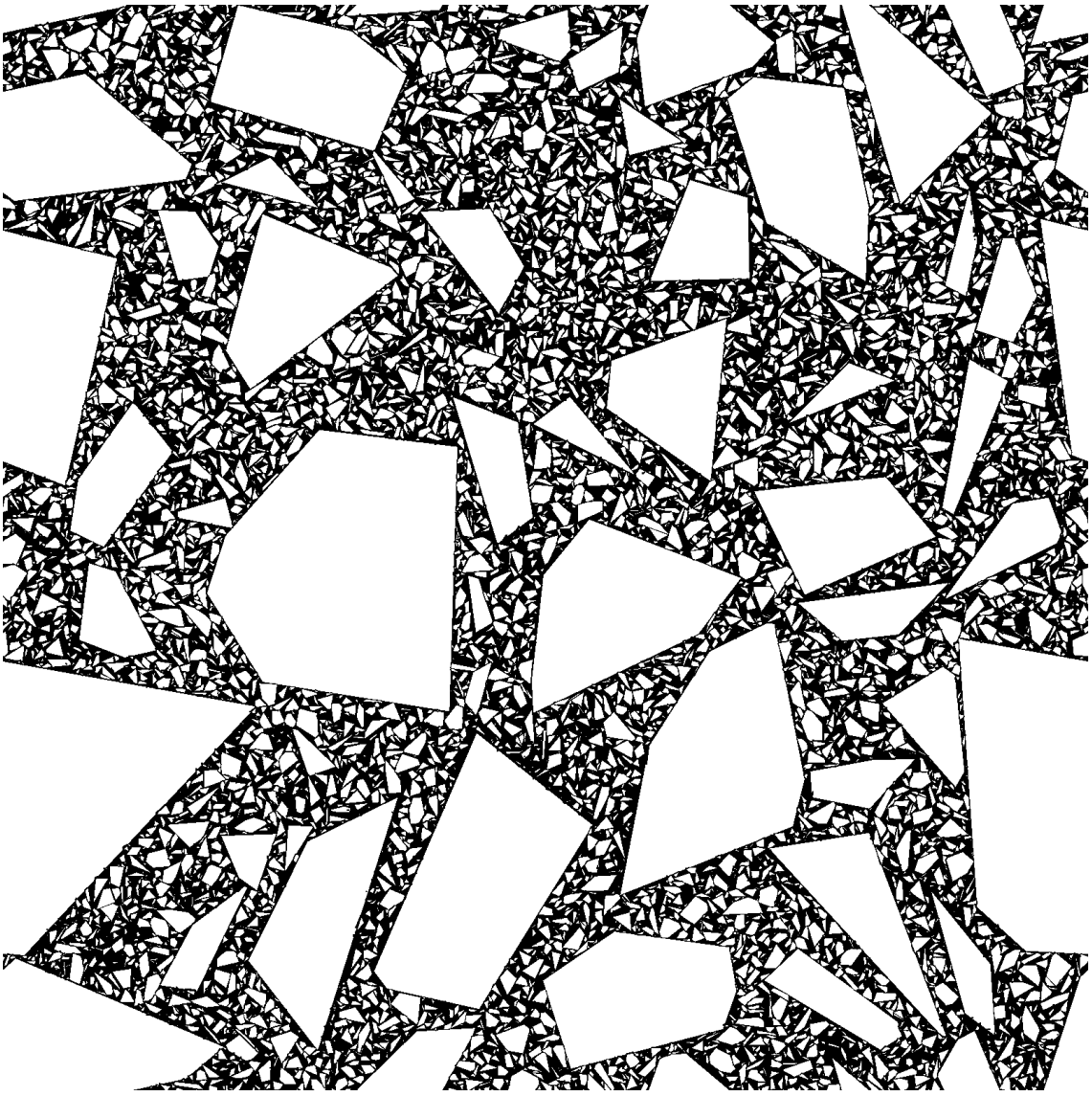


Figure 7: 2D section of the three-scales Poisson-polyhedra microstructure used to model the Biloba concrete.

Method	3-scales microstructure	Scales separation
$\widetilde{\kappa}/\kappa^c$	9.0	10.5
κ^+_{HS}/κ^c	30.6	
κ^-_{HS}/κ^c	8.3	
$V^{\kappa}_{5\%}$	2.5^3 cm^3 (280^3 voxels)	6.4^3 cm^3 (266^3 voxels)
$\widetilde{\mu}/\mu^c$	10.3	11.5
μ^+_{HS}/μ^c	30.8	
μ^-_{HS}/μ^c	8.6	
$V^{\mu}_{5\%}$	2.8^3 cm^3 (308^3 voxels)	7.3^3 cm^3 (303^3 voxels)

Table 3: FFT predictions for the effective elastic moduli $\widetilde{\kappa}$ and $\widetilde{\mu}$ of the Biloba concrete with contrast of properties $\chi = 100$ between the aggregates and cement paste. Column 2: full-fields computations on the 3-scales microstructure, column 3: computations involving two simplified microstructures and assuming scale separation. The RVE $V^{\kappa,\mu}_{5\%}$ for an error estimate of 5% are given for the two methods as well as the Hashin and Shtrikman bounds.

Biloba concrete. This difference represents a volume fraction of 4.5% of the cement paste. To overcome this, the elastic moduli in the cement paste are slightly increased by an amount corresponding to the Hashin and Shtrikman lower bounds.

Results for the effective elastic moduli of the Biloba concrete are given in Table (3), using the 3 scales microstructure or scale separation method. Hashin and Shtrikman bounds as well as RVEs for a relative precision of 5% are given for the two methods. The elastic moduli predicted for the Biloba concrete are higher when scale separation is assumed, by a relative amount of about 15%. This holds for both the bulk and shear moduli. Qualitatively similar results were obtained in (Willot & Jeulin, 2011) for multiscale Boolean models of spheres. in the problem considered in (Willot & Jeulin, 2011), the spheres are very stiff and aggregate into cluster. The multiscale Boolean model has stiffer elastic moduli when the ratio of the spheres diameter over the size of clusters increase, i.e. when scale separation holds.

5. Elastic properties of the Biloba concrete

This section focuses on the elastic properties of the 3-scales model for the Biloba concrete. The effective elastic moduli for the contrast of properties $\chi = 3$ and $\chi = 100$ are given in Tables (4) and (3), respectively. RVE sizes are given for a relative precision $\epsilon = 5\%$. Recall that the precision ϵ is related to the variance $D^2_{\sigma_{m,12}}(V)$ of the apparent moduli computed on a domain of size V by (Kanit et al., 2003, Escoda et al., 2011c):

$$\epsilon = \frac{2D_{\sigma_{m,12}}(V)}{\langle\sigma_{m,12}\rangle}, \qquad \frac{D^2_{\sigma_{m,12}}(V)}{D^2_{\sigma_{m,12}}} \sim A_3^{\sigma_{m,12}}\left(\frac{1}{V}-\frac{1}{V_0}\right), \quad V \gg A_3^{\sigma_{m,12}}, \tag{5}$$

where $A_3^{\sigma_{m,12}}$ and $D^2_{\sigma_{m,12}}$ are the integral range and point variances associated to the stress fields $\sigma_{m,12}$, and V are subdomains of the domain of computation V_0 of 1600^3 voxels. The volumes V must be much smaller than V_0, so that the term $1/V_0$ represents a lower-order correction in the asymptotic expansion of $D^2_{\sigma_{m,12}}(V)$. The integral range is determined by fitting numerical data for $D^2_{\sigma_{m,12}}(V)$, for increasing volume sizes V (see Fig. 10).

Stress field histograms for the two stress components $\sigma_{m,12}$ with applied hydrostatic and shear strain loading $\varepsilon^0_{m,12} = 100\%$ are represented in Fig. (11). As shown in this figure, the tails of the histograms have much slower decrease for the contrast $\chi = 100$.

The contrast of properties of $\chi = 3$ gives the elastic moduli predicted by the FFT method for the Biloba concrete. The latter are, according to data provided in Table (4), $\widetilde{E} = 40.8$ GPa and $\widetilde{\nu} = 0.2$. This value is much stiffer than the experimental measurement $E^b = 28.7$ GPa. Hereafter, various hypothesis are investigated to explain the discrepancy.

First, the local elastic moduli of the aggregates and cement paste could be overestimated. According to (Granger, 1996), the values for the Young modulus in the aggregates and cement paste are with a good confidence in the intervals $[48; 75]$ and $[14.2; 18]$ GPa, respectively (Table 5). The Poisson ratio varies in the ranges $[0.15; 0.3]$ (aggregates) and

$\widetilde{\kappa}/\kappa^c$	2.04
κ^+_{HS}/κ^c	2.12
$V^{\kappa}_{5\%}$	2.5^3 cm^3 (280^3 voxels)
$\widetilde{\mu}/\mu^c$	2.04
μ^+_{HS}/μ^c	2.12
$V^{\mu}_{5\%}$	2.8^3 cm^3 (308^3 voxels)

Table 4: FFT predictions for the effective elastic moduli $\widetilde{\kappa}$ and $\widetilde{\mu}$ of the 3-scales Biloba concrete with contrast of properties $\chi = 3$, and Hashin and Shtrikman upper-bounds, and RVE sizes for a required relative precision of 5%.

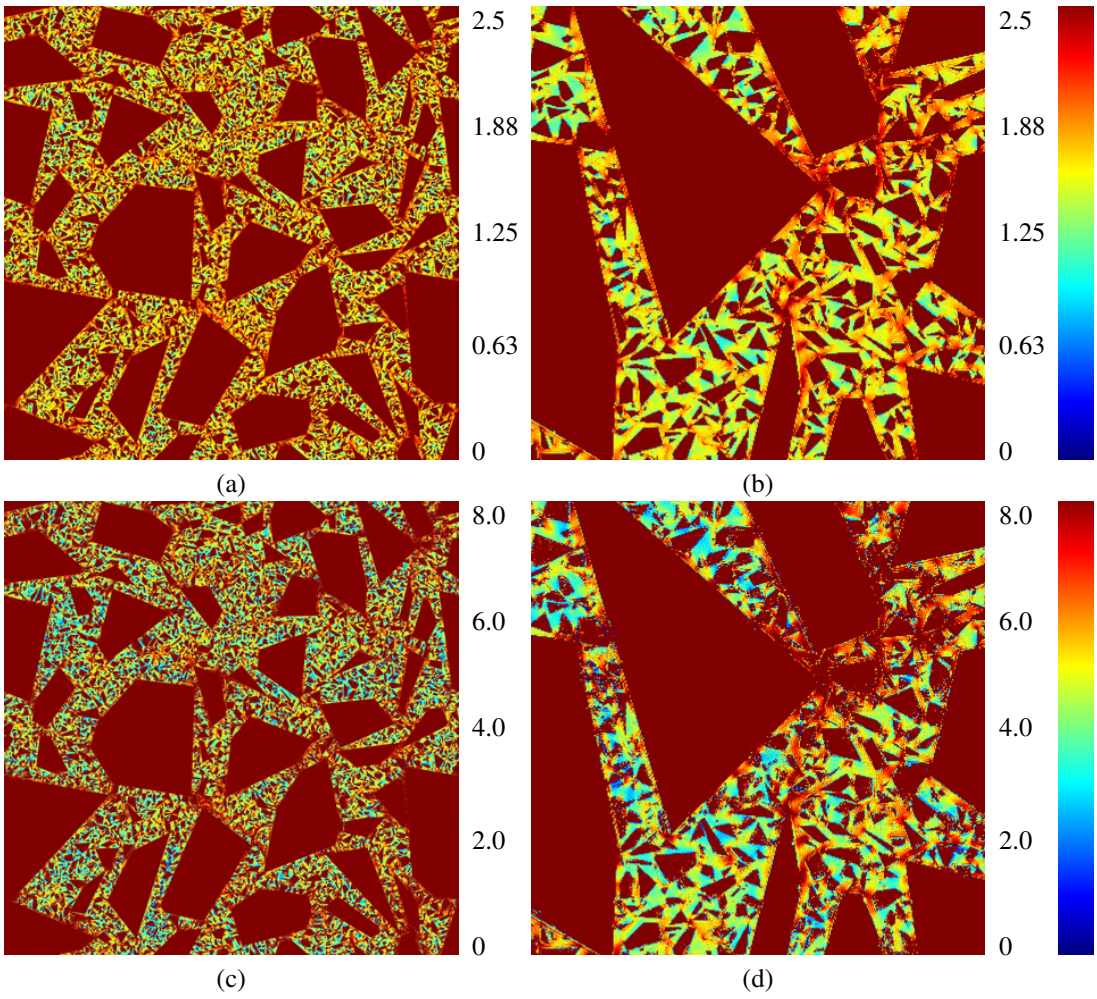


Figure 8: Maps of the normalized stress field $\sigma_m/\langle E^c\langle\varepsilon_m\rangle\rangle$ in the 3-scales model, for hydrostatic strain loading: contrast of properties $\chi = 3$ (a-b) and $\chi = 100$ (c-d). Maps (a) and (c): 1600^2 pixels, 14.4 cm 2D-sections, (b) and (d): 400^2 pixels, 3.6 cm enlargement. Color-scales are indicated on the right of each map.

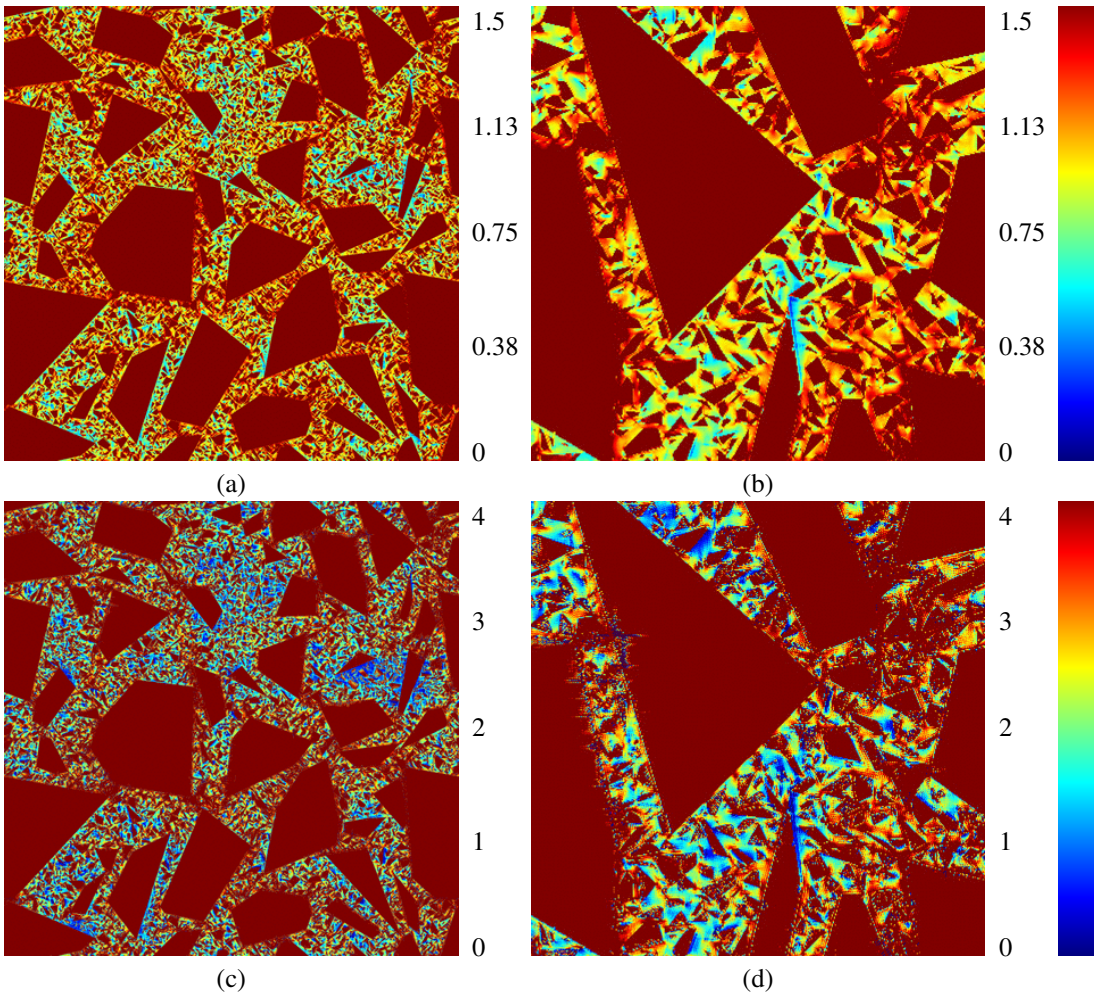


Figure 9: Continuation of Fig. (8): FFT maps for the shear stress field $\sigma_{12}/\langle E^g\langle\varepsilon_{12}\rangle\rangle$ in the 3-scales model, for shear strain loading: contrast of properties $\chi = 3$ (a-b) and $\chi = 100$ (c-d). Maps (a) and (c): 1600^2 pixels 2D-sections, (b) and (d): 400^2 pixels enlargement.

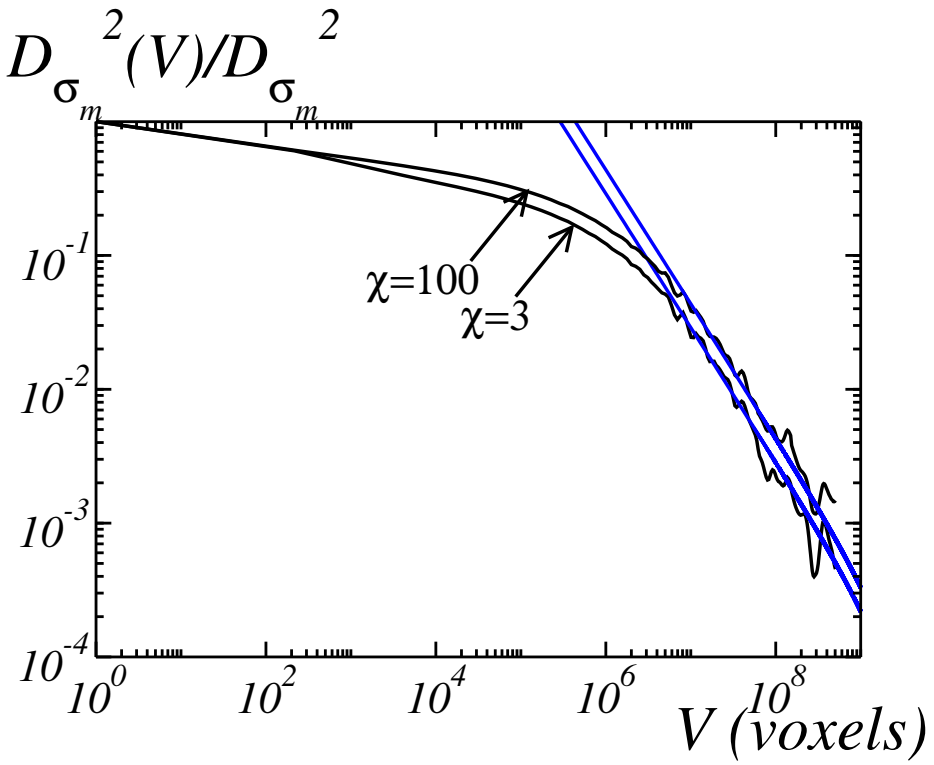


Figure 10: Normalized variance $D^2_{\sigma_m}(V)/D^2_{\sigma_m}$ of the apparent bulk modulus of the 3-scales model vs. volume size V for a contrast of properties $\chi = 3, 100$ (black curves). Blue curves: fit $D^2_{\sigma_m}(V)/D^2_{\sigma_m} \sim 1/V - 1/V_0$ for large volume sizes $V \gg A_3$.

	ν		E (GPa)	
	Min	Max	Min	Max
Aggregates	0.15	0.3	48	75
Cement paste	0.19	0.28	14.2	18

Table 5: Range of admissible values for the Poisson ratio and Young moduli in the cement paste and aggregates.

$[0.19; 0.28]$ (cement paste). The experimental measurement for the bulk modulus of the Biloba concrete is $\kappa^b = 15.9$ GPa. We first assume that the elastic moduli measured for the cement paste are correct and fix these. We then look for the values of the elastic moduli in the aggregates E^g and ν^g such that the lower Hashin and Shtrikman bounds recover the experimental measurement $\kappa^b = 15.9$ GPa (Table 6). The results are incompatible with the experimental measurements: the Young modulus is always larger than 42 GPa, which is significantly higher than the minimum value of 48 GPa (Table 5) and of the experimental measurement of 61.4 GPa. The reverse study is carried out in Table (7): the elastic moduli in the aggregates are fixed to their experimental values, and that of the cement paste are computed so that the Hashin and Shtrikman lower bounds recover the experimental moduli for the Biloba concrete. Again, the Young modulus E^c is always larger than 8, which is significantly lower than the minimum value of 14.2 (Table 5) and lower than the experimental measurement of 18 GPa. Thus, overestimation of the local properties can not explain the overestimation of the FFT predictions.

Second, we investigate if the presence of a porosity not accounted for in the cement paste explains the discrepancy between FFT predictions and measurements. The porosity in the cement paste and Biloba concrete have been measured (Sémétée et al., 2010) and are respectively 39.7% and 18.8%. Of the latter, 12.4% lies in the cement paste and 6.4% in the aggregates, or in-between aggregates and cement paste. We take into account the additional porosity by computing the upper Hashin and Shtrikman bound of a porous material with 6.4% of voids embedded in a matrix with elastic properties previously computed by FFT for $\chi = 3$. The effective elastic moduli are $\kappa^+_{HS} = 19.7$, $\mu^+_{HS} = 14.8$ and

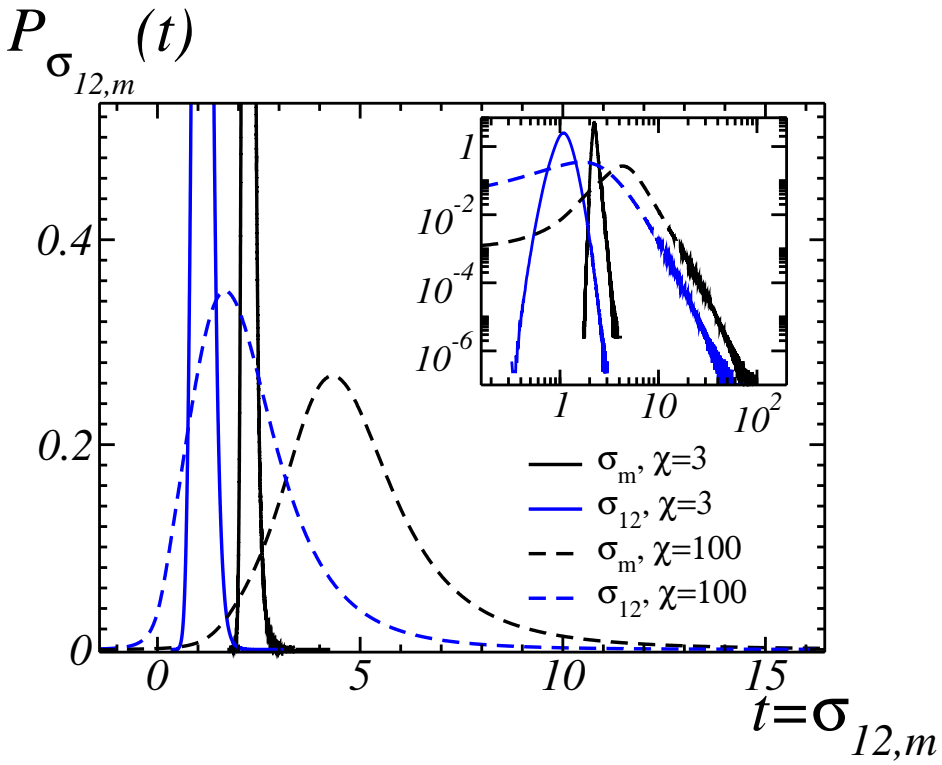


Figure 11: Stress field histograms $P_{\sigma_{m,12}}(t)$ for the stress components $\sigma_{m,12}$ in the cement paste, with contrast of properties $\chi = 3, 100$, in the 3-scales model, for applied strain loading $\varepsilon^0_{m,12} = 100\%$. Top-right graph: log-log plot of the same histograms.

ν^g	0.15	0.2	0.28
E^g (GPa)	42	36	26.4

Table 6: Values of the elastic moduli in the aggregates ν^g and E^g, such that the Hashin and Shtrikman lower bound recovers experimental measurements. The elastic moduli in the cement paste ν^c and E^c are fixed to their experimental values.

$E = 35.5$ GPa. This result is still much stiffer than the experimental measurement of $E^b = 28.7$ GPa.

Third, the effect of volume fraction of aggregates is investigated. The volume fraction of aggregates is, according to a segmentation of the micro-tomography of the Biloba concrete detailed in (Escoda et al., 2015), 45.1%. This value is thought to be underestimated. The Hashin and Shtrikman bounds for the effective elastic moduli of the Biloba concrete with 45.1% of aggregates are $18.2 < \kappa < 21.2$ and $12.1 < \mu < 13.4$ (GPa). These inequalities are incompatible with experimental measurement $\kappa^b = 16.0$ and $\mu^b = 12.0$ GPa.

6. Conclusion

Results obtained in this work are twofold. First, the shape of the aggregates have a strong influence on the local stress field, notably their distribution in the cement paste, when the contrast of properties between aggregates and

ν^c	0.19	0.25	0.28
E^c (GPa)	8	7	6.4

Table 7: Values of the elastic moduli in the cement paste ν^c and E^c, such that the Hashin and Shtrikman lower bound recovers experimental measurements. The elastic moduli in the aggregates ν^g and E^g are fixed to their experimental values.

cement paste is high. These differences are notable for the tails of the histograms which quantify the occurrences of highest stress. Such highest stress fields are located preferentially along the interface between cement paste and aggregates, where local debonding occurs. To a less extent, the aggregates shapes also influence the effective shear modulus. The effective bulk modulus is, however, quite insensitive to the particles shape.

The consequences of the scale-separation hypothesis between small and large aggregates was examined using full-field numerical predictions. The latter leads to quite stiffer predictions than that computed in materials with continuous granulometry for the aggregates.

Finally, FFT predictions were compared to experimental measurements in the linear elastic regime. The former are much stiffer than the measurements. Some possible explanations including overestimation of the microscopic elastic moduli, porosity not accounted for, wrong aggregates volume fraction, were ruled out. This leaves, among possible explanations, the effect of imperfect weak interfaces between aggregates and cement paste, for which models have been proposed (Hashin & Monteiro, 2002).

Acknowledgments

The authors are grateful to EDF for the financial support of this study (grant 47510).

References

References

Z. Chunsheng, K. Li, F. Ma, Numerical and statistical analysis of elastic modulus of concrete as a three-phase heterogeneous composite, Computers & Structures (139) (2014) 33–42. 1

C. Dunant, B. Bary, A. Giorla, C. Péniguel, J. Sanahuja, C. Toulemonde, A. Tran, F. Willot, J. Yvonnet, A critical comparison of several numerical methods for computing effective properties of highly heterogeneous materials, Advances in Engineering Software 58 (2013) 1–12. 4, 6

J. Escoda, D. Jeulin, F. Willot, Simulation of 3D granular media by multiscale random polyhedra, in: Proceedings of the International Congress of Stereology (ICS11), Beijing, 2011a. Online pre-print: `https://hal.archives-ouvertes.fr/hal-00879260`. 1, 2

J. Escoda, F. Willot, D. Jeulin, J. Sanahuja, C. Toulemonde, 3D morphological analysis of local elastic fields in a cementitious material, in: Advances in Structural Engineering and Mechanics (ASEM11), Seoul, 2011b. Online pre-print: `https://hal.archives-ouvertes.fr/hal-00879268`. 1, 5

J. Escoda, F. Willot, D. Jeulin, J. Sanahuja, C. Toulemonde, Estimation of local stresses and elastic properties of a mortar sample by FFT computation of fields on a 3D image, Cement and Concrete Research 41 (5) (2011c) 542–556. 1, 5, 6, 10

J. Escoda, Modélisation morphologique et micromécanique 3D de matériaux cimentaires, Ph.D. thesis, École nationale supérieure des mines de Paris (2012). 1, 2

J. Escoda, D. Jeulin, F. Willot, C. Toulemonde, 3D morphological modeling of concrete using multiscale poisson polyhedra, Journal of Microscopy 258 (1) (2015) 31–48. 1, 2, 4, 7, 14

L. Granger, Comportement différé du béton dans les enceintes de confinement de centrales nucléaires, analyse et modélisation d'ouvrage, Ph.D. thesis, Laboratoire Central des Ponts et Chaussées (1996). 2, 3, 10

Z. Hashin, P. Monteiro, An inverse method to determine the elastic properties of the interphase between the aggregate and the cement paste, Cement and Concrete Research 32 (8) (2002) 1291–1300. 15

Z. Hashin, S. Shtrikman, A variational approach to the theory of the elastic behaviour of multiphase materials, Journal of the Mechanics and Physics of Solids 11 (2) (1963) 127–140. 6

H. He, P. Stroeven, M. Stroeven, L. Sluys, Influence of particle packing on elastic properties of concrete, Magazine of Concrete Research 64 (2) (2011) 163–175. 1

T. Kanit, S. Forest, I. Galliet, V. Mounoury, D. Jeulin, Determination of the size of the representative volume element for random composites: statistical and numerical approach, International Journal of Solids and Structures 40 (13–14) (2003) 3647–3679. 6, 10

C. Lantuéjoul, Skeletonization in quantitative metallography, Issues of Digital Image Processing 34 (1980) 107–135. 5

A. Legrix, Projet biloba : élaboration d'éprouvettes de béton et de pâte cimentaire pour l'étude expérimentale de l'influence de l'humidité sur la vitesse de fluage des bétons, ÉDF R&D internal report (2009). 2

J.-C. Michel, H. Moulinec, P. Suquet, A computational method based on augmented lagrangians and fast fourier transforms for composites with high contrast, Computer Modelling in Engineering & Sciences 1 (2) (2000) 79–88. 3

N. Reviron, Étude du fluage des bétons en traction. applications aux enceintes de confinement des centrales nucléaires à eau sous pression, Ph.D. thesis, École Normale Supérieure de Cachan (2009). 2

J. Sanahuja, C. Toulemonde, Numerical homogenization of concrete microstructures without explicit meshes, Cement and Concrete Research 41 (2011) 1320–1329. 3

P. Sémété, B. Février, M. Hervé, A. Legrix, Projet biloba : courbe de désorption des bétons de type civaux b11 – essais sur lames minces à 25° c, rapport interne EDF R&D (2010). 13

J. Shilstone, Concrete misture optimization, Concrete International 12 (6) (1990) 33–39. 1

P. Soille, Generalized geodesy via geodesic time, Pattern Recognition Letters 15 (12) (1994) 1235–1240. 5

F. Willot, Fourier-based schemes for computing the mechanical response of composites with accurate local fields, Comptes rendus de l'Académie des Sciences: Mécanique 343 (3) (2015) 232–245. 1, 6

F. Willot, L. Gillibert, D. Jeulin, Microstructure-induced hotspots in the thermal and elastic responses of granular media, International Journal of Solids and Structures 50 (10) (2013) 1699–1709. 6

F. Willot, D. Jeulin, Elastic and electrical behavior of some random multiscale highly-contrasted composites, International Journal for Multiscale Computational Enginneering: special issue on Multiscale modeling and uncertainty quantification of heterogeneous materials 9 (3) (2011) 305–326. 10

P. Wriggers, S. Moftah, Mesoscale models for concrete : Homogenisation and damage behaviour, Finite Elements in Analysis and Design 42 (2006) 623–636. 2, 3